

Single-Cell Clustering via Dual-Graph Alignment

Dayu Hu, Ke Liang, and Xinwang Liu, *Senior Member, IEEE*

Abstract—In recent years, the field of single-cell RNA sequencing has seen a surge in the development of clustering methods. These methods enable the identification of cell subpopulations, thereby facilitating the understanding of tumor microenvironments. Despite their utility, most existing clustering algorithms primarily focus on the attribute information provided by the cell matrix or the network structure between cells, often neglecting the network between genes. This oversight could lead to loss of information and clustering results that lack clinical significance. To address this limitation, we develop an advanced single-cell clustering model incorporating dual-graph alignment, which integrates gene network information into the clustering process based on self-supervised and unsupervised optimization. Specifically, we designed a graph-based autoencoder enhanced by an attention mechanism to effectively capture relationships between cells. Moreover, we performed the node2vec method on Protein-Protein Interaction (PPI) networks to derive the gene network structure and maintained this structure throughout the clustering process. Our proposed method has been demonstrated to be effective through experimental results, showcasing its ability to optimize clustering outcomes while preserving the original associations between cells and genes. This research contributes to obtaining accurate cell subpopulations and generates clustering results that more closely resemble real-world biological scenarios. It provides better insights into the characteristics and distribution of diseased cells, ultimately building a foundation for early disease diagnosis and treatment.

Index Terms—Gene map, Clustering, Protein-protein interaction, Node2vec, Deep learning.

I. INTRODUCTION

Single-cell transcriptome sequencing technology is a powerful tool for investigating the origins and microenvironments of tumors[1], [2], [3], [4]. The clustering process of cells is a crucial step in which cells can be divided into different subtypes based on the analysis of signal patterns between them. These subtypes can provide valuable insights for clinical treatment.

In recent years, there has been a significant increase in the development of clustering algorithms designed for single cell RNA sequencing(scRNA) data[5], [6]. Early approaches relied on probabilistic models that estimated high-dimensional cell data by computing the probability of gene expression. For instance, CIDR[7] proposed an interpolation method to handle dropout events, while SC3[8] used hierarchical Kmeans clustering to perform consensus clustering assuming Euclidean relationships between cells. However, these methods make the assumption that biological data is linear and clear, which may not always hold true in the real world.

To effectively extract features from scRNA data and evade assumptions about data distribution, some researchers have suggested that neural networks could be a promising approach to mining information from scRNA data[9], [10]. The neural network is a widely used black box model that can

fit almost all data distributions if the parameter setting is appropriately set. Numerous deep clustering algorithms have been proposed to obtain effective representations, including the popular framework DESC[11], which iteratively learns the gene expression pattern of each cluster, assigns cells to their respective clusters, and continuously eliminates batch effects. Another impressive work is scDeepCluster[12], a method based on the Zero-inflated Negative Binomial(ZINB) model that uses a bottleneck layer for deep k-means clustering to improve clustering results. However, these models treat cells as isolated individuals, ignoring the associations between them.

To incorporate cellular interaction relationships into the clustering process, some researchers have proposed a graph-based approach for learning cell embeddings. This entails constructing a cell graph through the similarity between cells. Seurat[13] is a well-known method that uses Louvain community detection to construct a cell graph, which is then subjected to spectral clustering using Phenograph. In terms of graph-based deep clustering, scGNN[14] uses a graph neural network to capture and aggregate the relationships between cells, and a Gaussian model to simulate the pattern of heterogeneous gene expression. In addition, scGAC[15] introduces attention mechanisms based on the cell-to-cell graph to ensure effective information transmission between cells. scDFC[16] combines structural information derived from cell-to-cell graphs and attribute information obtained from cellular expression patterns, enabling a comprehensive analysis of scRNA data.

Although numerous clustering approaches primarily concentrate on the expression of cells themselves or the cell-to-cell graph connecting them, few studies emphasize the connections between genes. In reality, genes within each cell engage in intricate interrelationships stemming from interactions, regulatory mechanisms, or shared functions and pathways in biological processes. In essence, a gene-to-gene graph exists, yet it remains unexplored in the field of scRNA clustering. By constructing a gene-to-gene graph and modeling the relationships between genes, we can significantly optimize the clustering embedding and enhance the clustering results. Furthermore, this embedding might lead to more accurate representations of biological features, thereby improving the consistency between the identified clusters and the actual underlying biological systems.

Based on these considerations, we developed an effective single-cell clustering model via dual-graph alignment(SCC-DGA), which simultaneously focuses on the cell-to-cell graph and gene-to-gene graph. To accomplish this, we utilized a graph attention autoencoder to capture the relationships between cells and ensure effective information transmission between them. In addition, we performed random walks on the protein-protein interaction(PPI) network corresponding to the gene set to obtain the embedding of the gene-to-

gene graph, while maintaining the consistency of this gene graph during the clustering process. Experiments on eight real scRNA datasets demonstrate that the SCC-DGA method is stable and outperforms the other nine baseline methods. Our contributions can be summarized as follows:

- The SCC-DGA model simultaneously focuses on the cell-to-cell graph and gene-to-gene graph, fusing them and aligning these structures during the clustering process to generate more effective clustering results.
- The SCC-DGA model employs a dual-supervised module to facilitate the optimization of the bottleneck layer. effectively utilizes its own information and requires no exogenous labels.
- The SCC-DGA model is robust and outperforms the other nine baseline methods.

II. MATERIALS AND METHODS

A. Datasets

This study introduces eight real-world datasets from common species, including humans and mice. To measure the performance of different clustering algorithms, all datasets are attached to authoritative labels. And here is a brief introduction for each dataset:

- **Biase**[17] is a representative small scRNA dataset and primarily derived from mice. It consists of embryonic cells collected during the developmental stages of mice.
- **Darmanis**[18] contains human brain cells, which are known to have a more complex composition. As a result, this dataset has been divided into multiple clusters.
- **Enge**[19] consists of pancreatic cells from the human species.
- **Bjorklund**[20] is another dataset from the human species, consisting of lymphoid cells that play a crucial role in the immune system.
- **Sun**[21] released three single-cell datasets on their Github repository, and in this work we selected the first one, which only contains mouse lung cells.
- **Marques**[22] comprises data from mice and was specifically collected to investigate the developmental origin of oligodendrocyte precursor cells.
- **Zeisel**[23] comprises data from mice collected from the regions of the somatosensory cortex and hippocampus CA1.
- **Fink**[24] is from the human species. It was collected from the adult ureter, which might pass insights into metabolic processes.

The initial scRNA data display considerable variability in scale and elevated noise levels, potentially leading to false conclusions in subsequent analyses. To address these concerns, we conducted quality control on the cellular data before proceeding with clustering. Specifically, we retained cells with expression values within a reasonable range and eliminated outlier cells exhibiting extreme expression values. And we achieved this by establishing upper and lower thresholds at 75% plus three times the quartile deviation, and 25% minus the quartile deviation, respectively. After quality control, we

TABLE I
DETAILS OF THE EIGHT REAL DATASETS

Datasets	Genes	Clusters	References
Biase	21489	3	[17]
Darmanis	9337	8	[18]
Enge	25929	9	[19]
Bjorklund	26087	4	[20]
Sun	995	6	[21]
Marques	15291	14	[22]
Zeisel	18825	9	[23]
Fink	20932	7	[24]

standardized the data by scaling it to a consistent range. Next, we applied a log2 transformation to the data. To prevent negative infinite values and guarantee the expression value is always positive, we incorporated a pseudo count of 1 during the transformation process.

B. The framework of SCC-DGA

Figure 1 depicts the comprehensive workflow of the SCC-DGA model, which consists of two main modules.

The first module is the dual-graph alignment module. This module processes the cell dataset and gene set in parallel to construct two separate graphs: the cell-to-cell graph and the gene-to-gene graph. To construct the cell-to-cell graph, a k-nearest neighbors (KNN) approach based on similarity measures is employed, and then a specific adjacency matrix is obtained. This adjacency matrix, along with the reduced cell matrix, is then fed into a graph attentional autoencoder, as shown in the figure. On the other hand, to construct the gene-to-gene graph, exogenous information is used. Specifically, the gene set is input into the online STRING website to generate a PPI network corresponding to the gene set. This network is then fed as the input of the node2vec algorithm to perform random walks and obtain the final graph.

The second module of the model is the dual-supervised optimization module. This module benefits from two supervised mechanisms and relies on no external labels. Initially, the structures of the cell-to-cell graph and the gene-to-gene graph are obtained. Then, a self-supervised mechanism is used to constrain the stability of these two graphs during the embedding optimization process. Additionally, the shared bottleneck layer is optimized with an unsupervised mechanism to ensure that the embedding exhibits exceptional clustering performance.

C. Dual-graph fusion module

This section provides a detailed description of the dual-graph fusion module, including the definition of formulas for dual-graph graphs and the specific computational procedure.

1) *Cell-to-cell graph*: To accurately learn the cell-to-cell graph information, we designed a graph-based autoencoder(GAT) enhanced by an attention mechanism to fully capture the cell signaling patterns and cell-to-cell relationships. The input feature matrix X_{cell} is encoded to produce the cell embedding Z_{cell} , which is obtained with the following equation:

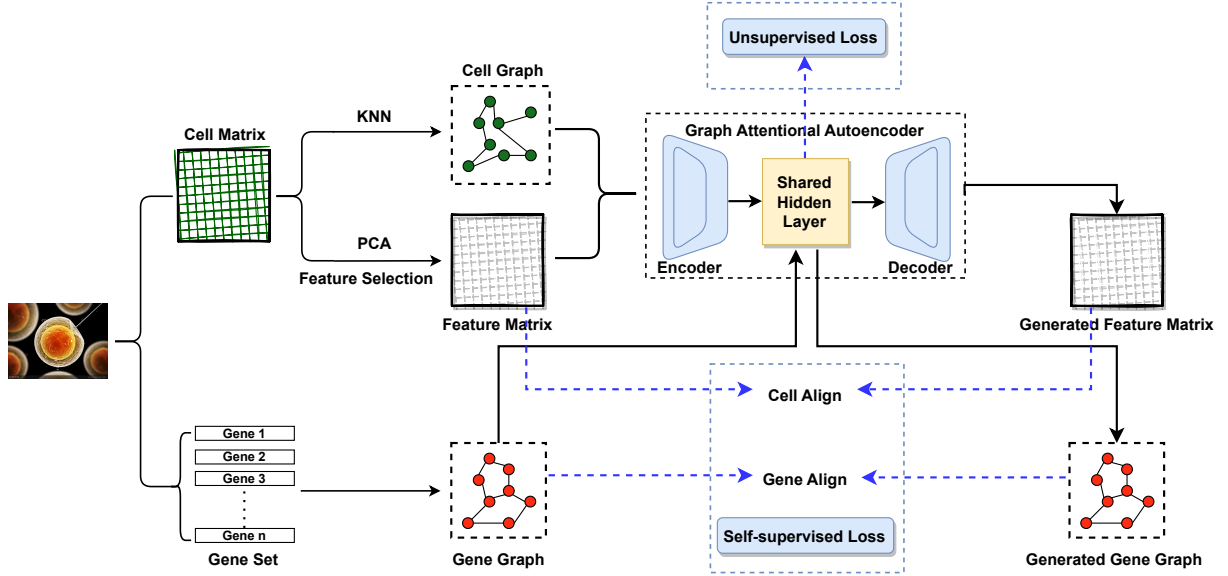


Fig. 1. Illustration of the data processing and framework of SCC-DGA.

$$\mathbf{Z}_{cell} = \sigma(\mathbf{W}_E \mathbf{X}_{cell}) \quad (1)$$

The encoding weight parameter matrix W_E in GAT is composed of learnable parameters that map the input to the bottleneck layer. During training, each element of W_E can be adjusted. The nonlinear activation function σ enables the neural network to learn complex patterns and features.

The embedding Z_{cell} obtained from GAT is then fused with the embedding generated from the gene-to-gene graph, denoted as Z_{gene} . This process is performed as follows:

$$\mathbf{Z}_F = \sigma([\mathbf{Z}_{cell} || \mathbf{Z}_{gene}]) \quad (2)$$

The shared embedding of the two graphs is denoted by Z_F , and the concatenation operation is denoted by $||$. The nonlinear activation function σ is the same as described above.

Next, the decoding module reconstructs the shared embedding, which can be expressed as:

$$\mathbf{X}'_{cell} = \mathbf{W}_D \mathbf{Z}_F \quad (3)$$

where W_D is the learnable decoding matrix of GAT.

2) *Gene-to-gene graph*: This section provides a detailed guide on how to build a gene-to-gene graph from a single-cell dataset.

To begin, we preprocessed each single-cell dataset by using Scanpy to screen for highly variable genes. We kept the top 2000 genes as the final gene set. Next, we input the gene set into the online platform STRING¹ to construct a PPI network. We saved the network as an adjacency table to perform the following random walk.

To generate node embeddings for the PPI network, we employ a biased approach node2vec to perform random walk, which involves two neighborhood approaches, namely

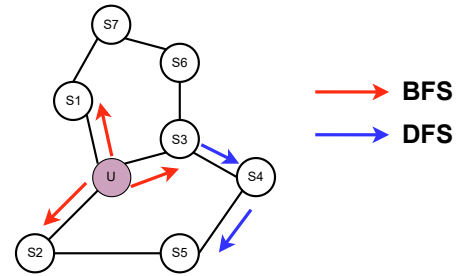


Fig. 2. In BFS and DFS traversals, the node pointed to by the red line is considered a low-order neighbor of the source node, while the node pointed to by the blue line is considered a higher-order neighbor.

breadth-first search (BFS) and depth-first search (DFS). The BFS prioritizes walking toward nodes of the same order, while DFS prioritizes walking toward higher-order nodes. Figure 2 illustrates the specific procedure of random walks. By utilizing these two strategies, node2vec can achieve effective walks, resulting in better node embeddings.

Formally, let $G = (V, E)$ be a PPI network, where V represents the set of nodes corresponding to proteins, and E denotes the interactions between them. We employ node2vec to obtain an embedding vector for each node. Specifically, We treat the sequence S_v as a corpus and use the skip-gram model to capture the features. The skip-gram model aims to maximize the probability of observing the node v in a given context. Therefore, for node v , we maximize the following likelihood function:

$$\frac{1}{|S_v|} \sum_{u \in S_v} \sum_{j \in \mathcal{N}_u} \log P(v_j | v_u) \quad (4)$$

Here, \mathcal{N}_u denotes the set of neighboring nodes of node u , and $P(v_j | v_u)$ is the conditional probability of node j given node u . The softmax function is used to calculate this probability, which is defined as follows:

¹<https://www.string-db.org/>

$$P(v_j|v_u) = \frac{\exp(\mathbf{v}_j^\top \mathbf{v}_u)}{\sum_k k \in V \exp(\mathbf{v}_k^\top \mathbf{v}_u)} \quad (5)$$

Here, \mathbf{v}_u and \mathbf{v}_j are the embedding vectors of nodes u and j , respectively. We assume that there are n nodes in the PPI network, The gene embedding X_{gene} can be obtained as below:

$$\mathbf{X}_{gene} = [\mathbf{v}_1, \mathbf{v}_2, \dots, \mathbf{v}_n]^\top \quad (6)$$

The node embeddings of the PPI network are fed into a neural network for joint training, and then reconstructed through a decoder. The training process can be defined as:

$$\mathbf{Z}_{cell} = \sigma(\widetilde{\mathbf{W}}_E \mathbf{X}_{gene}) \quad (7)$$

where \mathbf{W}_E is the learnable encoding matrix of gene-to-gene graph, and σ is the nonlinear activation function.

Similarly, we compute the gene-to-gene graph using the following equation:

$$\mathbf{X}'_{gene} = \widetilde{\mathbf{W}}_D \mathbf{Z}_F \quad (8)$$

where \mathbf{W}_D is the learnable decoding matrix of gene to gene graph.

D. Dual-Supervised Optimization Module

1) *Self-supervised Optimization*: The objective of self-supervised optimization is to leverage the inherent features of the data itself. In SCC-DGA, we used the self-supervised loss to constrain the structure of the cell-to-cell graph and gene-to-gene graph, maintaining the stability of both graphs during the embedding optimization process. Specifically, we achieved this by aligning the original input data with the reconstructed data.

For the cell-to-cell graph, we aimed to obtain a reconstructed cell matrix that is similar to the previous matrix. To achieve this, we employed cosine loss, a commonly used similarity measurement, to constrain the similarity during the clustering process, as shown below:

$$L_{cell} = \frac{\mathbf{X} \cdot \mathbf{X}'_{cell}}{\|\mathbf{X}\| \cdot \|\mathbf{X}'_{cell}\|} \quad (9)$$

For the gene-to-gene graph, we tried to keep reconstructed gene data unchanged. To achieve this, we employed Mean Absolute Error(MAE) loss to ensure that the genes remain functionally intact during the optimization process of clustering. The specific alignment process is as follows:

$$L_{gene} = \left| \mathbf{X}_{gene} - \widetilde{\mathbf{W}}_D \sigma(\widetilde{\mathbf{W}}_E \mathbf{X}_{gene}) \right| \quad (10)$$

The final self-supervised loss is combined as below:

$$L_{ssl} = 2\lambda L_{cell} + 2(1 - \lambda)L_{gene} \quad (11)$$

Where λ is a tunable hyperparameter.

2) *Unsupervised Optimization*: In this work, we employed the student's t-distribution to optimize the bottleneck layer. The matrix Q stored the cluster assignment of each cell, as below:

$$q_{ij} = \frac{\left(1 + \|\mathbf{z}_i - \mathbf{u}_j\|^2\right)^{-1}}{\sum_{k=1}^c \left(1 + \|\mathbf{z}_i - \mathbf{u}_k\|^2\right)^{-1}} \quad (12)$$

where z was the embedding of cell, u denoted the center of clustering. And then we built auxiliary target distribution P based on clustering distribution Q .

$$p_{ij} = \frac{q_{ij}^2 / \sum_{i=1}^n q_{ij}}{\sum_{k=1}^c (q_{ik}^2 / \sum_{i=1}^n q_{ik})} \quad (13)$$

The goal of optimizing Q is to make it as close as possible to P , so we employed the KL divergence to constrain them, namely unsupervised loss, denoted as below:

$$L_{ul} = \sum_{i=1}^c \sum_{j=1}^n p_{ij} \log \frac{p_{ij}}{q_{ij}} \quad (14)$$

To summarize, the dual-supervised optimization module employs a two-step learning strategy that consists of self-supervised optimization based on the data itself, and unsupervised optimization based on the t-distribution of students.

The self-supervised optimization is achieved through dual-graph alignment, which maintains the structure of cell-to-cell and gene-to-gene graphs during clustering and helps to learn a meaningful compressed representation.

The unsupervised optimization aims to minimize the distance between the real clustering assignment and the auxiliary target clustering distribution, thereby generating embeddings that exhibit high clustering performance.

By combining these two optimization modules, the total loss of our model has been formulated as below:

$$L = L_{ssl} + L_{ul} \quad (15)$$

E. Evaluation metrics

Three evaluation metrics are involved in this work:

- **Adjusted Rand Index(ARI)**[25]

ARI represents a commonly used measure of the consistency between clustering results and true labels, and it requires labeled data. This index can be formulated as below:

$$ARI = \frac{\sum_{ij} \binom{n_{ij}}{2} - [\sum_i \binom{a_i}{2} \sum_j \binom{b_j}{2}] / \binom{n}{2}}{\frac{1}{2} [\sum_i \binom{a_i}{2} + \sum_j \binom{b_j}{2}] - [\sum_i \binom{a_i}{2} \sum_j \binom{b_j}{2}] / \binom{n}{2}} \quad (16)$$

- **Normalized Mutual Information (NMI)**[26]

NMI represents another commonly used measure of the similarity between clustering results and true labels, and it also requires labeled data. This index can be formulated as below:

TABLE II
ARI SCORE OF SCC-DGA AND BASELINE METHODS ON EIGHT DATASETS, THE RED VALUE INDICATES THE TOP 3 RESULTS.

Dataset	CIDR	SC3	scDeepCluster	DESC	scGNN	Seurat	scAE	scGAC	SCDFC	SCC-DGA
Biase	1.000	0.948	0.948	0.960	0.330	0.850	1.000	1.000	1.000	1.000
Darmanis	0.337	0.470	0.522	0.536	-	0.353	0.1	0.508	0.533	0.549
Enge	0.223	0.531	0.218	0.305	-	0.206	0.052	0.261	0.368	0.483
Bjorklund	0.457	0.721	0.310	0.412	0.438	0.056	-	0.785	0.842	0.724
Sun	0.268	0.879	0.783	0.603	0.465	0.182	0.276	0.784	0.784	0.834
Marques	0.100	0.363	0.390	0.269	-	0.172	-	0.283	0.26	0.399
Zeisel	0.167	0.420	0.736	0.279	-	0.119	-	0.657	0.317	0.605
Fink	0.225	0.146	0.359	0.212	-	0.063	0.179	0.328	0.485	0.561

$$NMI = \frac{2MI(U, V)}{H(U) + H(V)} \quad (17)$$

• Silhouette Coefficient (SC)[27]

The SC is an internal evaluation metric that can assess the quality of clustering results in an unsupervised manner, without the need for ground truth labels. The range of SC is from -1 to 1, where a value of 1 indicates high compactness and good separation between clusters, a value of -1 indicates low compactness and poor separation between clusters, and a value of 0 indicates overlapping clusters. Unlike the previous two metrics, the SC provides a more comprehensive evaluation of the clustering results by taking into account both the within-cluster and between-cluster distances. In this work, we use it to control the early stop of our Python implementation.

$$s_i = \frac{b_i - a_i}{\max(a_i, b_i)} \quad (18)$$

F. Parameter setting

To evaluate the performance of our proposed algorithm, we conducted experiments on a Ubuntu server equipped with an Intel Core i7-6800K CPU, 64GB of DDR4 memory, and an NVIDIA TITAN Xp graphics card. The version of the system was Ubuntu 22.04.2 LTS, and we implemented the algorithm in Python 3.6 using the TensorFlow deep learning framework version 1.12.0.

For our SCC-DGA model, we set the parameters of the random walk on the gene-to-gene graph to the default parameters of the node2vec algorithm. The size of the encode layers was set to (512, 256, 64), and the bottleneck layer was set to 64. The model underwent a pre-training phase of 200 epochs, followed by a training phase of 5000 epochs. The learning rate for pre-training was set to 0.0002, and the learning rate for training was set to 0.0005.

III. RESULTS

A. SCC-DGA outperforms other nine baseline methods

Here, we design experiments to evaluate the effectiveness of current representative clustering methods, including our proposed SCC-DGA model and nine other baseline methods.

Next, we provide a brief description of each method included in this study and our rationale for their inclusion.

Additionally, we present a clear analysis of the experimental results.

- **CIDR**[7] employs a probabilistic model to evaluate dropout events in cellular data, which is regarded as a typical traditional clustering method in this paper.
- **SC3**[8] utilizes a consensus clustering strategy based on K-means clustering and Euclidean distance, which is regarded as a typical traditional clustering method in this paper.
- **scDeepCluster**[12] proposes a deep autoencoder that employs the zero-inflated negative binomial (ZINB) loss, which is regarded as a typical deep clustering method in this paper.
- **DESC**[11] also employs an autoencoder network to obtain the embedding of cells and eliminate batch effects, which is regarded as a typical deep clustering method in this paper.
- **scGNN**[14] integrates three iterative multimodal autoencoders based on graph neural networks, which is regarded as a typical graph deep clustering method in this paper.
- **Seurat**[13] includes a built-in Phenograph clustering method that constructs cell graphs using community detection, which is regarded as a typical graph clustering method in this paper.
- **scAE** is a simple deep clustering model we constructed for comparison, which is regarded as a typical deep clustering method in this paper.
- **scGAC**[15] introduces an attention mechanism on graph neural networks to efficiently build cellular graphs, which is regarded as a typical graph deep clustering method compared this paper.
- **scDFC**[16] fuses attribute information of cells and structural information between cells for clustering, which is regarded as a typical deep fusion clustering method in this paper.

Based on our results, it is evident that SCC-DGA consistently achieved excellent performance in terms of ARI, as shown in Table 2. It always ranked top three in all compared methods and ranked first in four out of eight datasets. To show visual results, we built a heat map based on clustering performance, as shown in Figure 3. Each number within the square reflects the magnitude of the ARI values, with the color gradient from blue-purple to yellow-green indicating the ARI values from low to high. Additionally, the sizes of each square

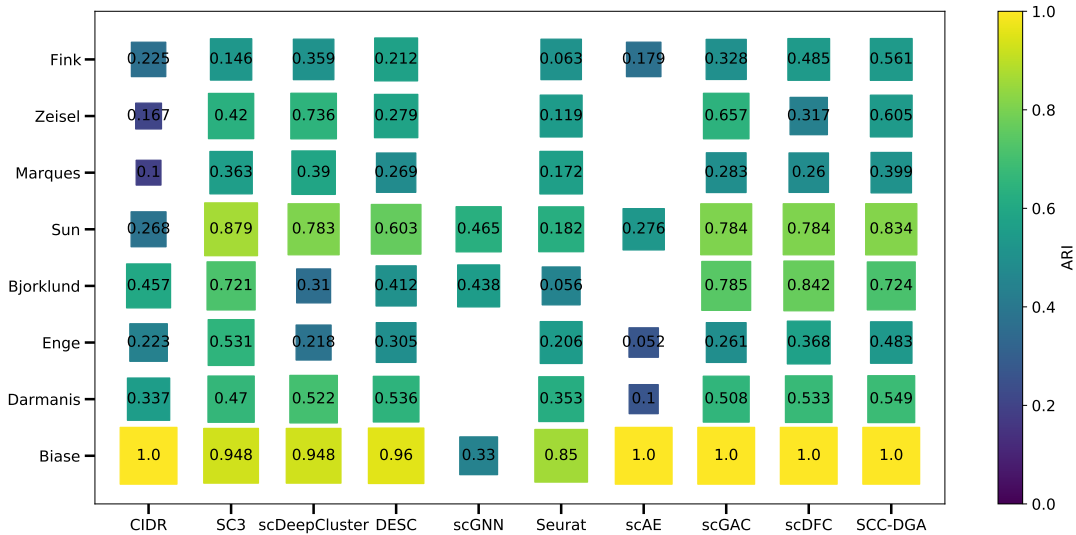


Fig. 3. The clustering performance of SCC-DGA is presented in the heatmap. Each number within the square represents the magnitude of the ARI values, with the color gradient ranging from blue-purple to yellow-green indicating ARI values from low to high. The size of each square indicates the results of NMI.

are indicative of the results of NMI. It is worth noting that CIDR, scDeepCluster, and scAE exhibited high volatility in terms of NMI.

In contrast, SCC-DGA not only demonstrated superiority in ARI, but also exhibited great stability in NMI. As single-cell data originates from a complex biological environment that involves rich metabolic reflections, it is challenging to find a general clustering method that is universally applicable to all cases. However, SCC-DGA exhibited high performance in almost all tasks.

B. SCC-DGA reveals that gene-to-gene graphs do indeed exist among genes

In this work, we propose a gene-to-gene graph that maps the relationships between genes. Its relatedness is obtained from protein expression. To obtain the corresponding protein-protein interaction (PPI) networks, we input the gene sets corresponding to the single-cell data into the well-known protein interaction network database, STRING. These PPI networks present the association relationships between genes.

To visually show this map, we performed gene mapping for each dataset by feeding the gene sets into the STRING database and obtaining the corresponding PPI adjacency matrices, which were then mapped using the software Cytoscape. The final result was presented in Figure 4.

As shown in Figure 4, there are eight gene-to-gene graphs from different scRNA datasets. It illustrates that the gene-to-gene graph does indeed exist, providing a real biological sense of interaction between genes, which can be used to study gene function, regulation, and disease mechanisms. Therefore, it is of potential scientific value to maintain the stability of the gene-to-gene graph during the clustering process.

C. SCC-DGA learns efficient clustering embedding

The quality of learned embeddings has a direct impact on the performance of clustering. In this section, we investigate whether SCC-DGA has learned great clustering embeddings and further explore the reasons behind it.

To evaluate the quality of clustering embeddings generated by SCC-DGA, we saved the bottleneck layer and visualized it using tSNE on the Sun dataset. The result in Figure 5 illustrates that SCC-DGA has learned excellent clustering embeddings, with well-assigned clusters and only a few instances of unclear clusters.

To further explore why SCC-DGA enables to learn excellent clustering embeddings, we conducted experiments to remove the GAT module and gene-to-gene graph module from the model, respectively. We found that the quality of the embeddings significantly declined without these modules. Specifically, as highlighted in the red box in Figure 5, the removal of the gene map led to a small number of cells not being clearly assigned to the right clusters. These results suggest that the GAT module and gene map module used in SCC-DGA play a crucial role in establishing excellent cluster embeddings, with both modules contributing to high-quality embeddings.

D. Parameter fine-tuning

In this work, we highlight the significant impact of dual-graph alignment on clustering performance and propose a weight coefficient, denoted as λ , to control the weights of the cell-to-cell graph and gene-to-gene graph. In this section, we provide a detailed analysis of the hyperparameter λ and its effect on clustering performance.

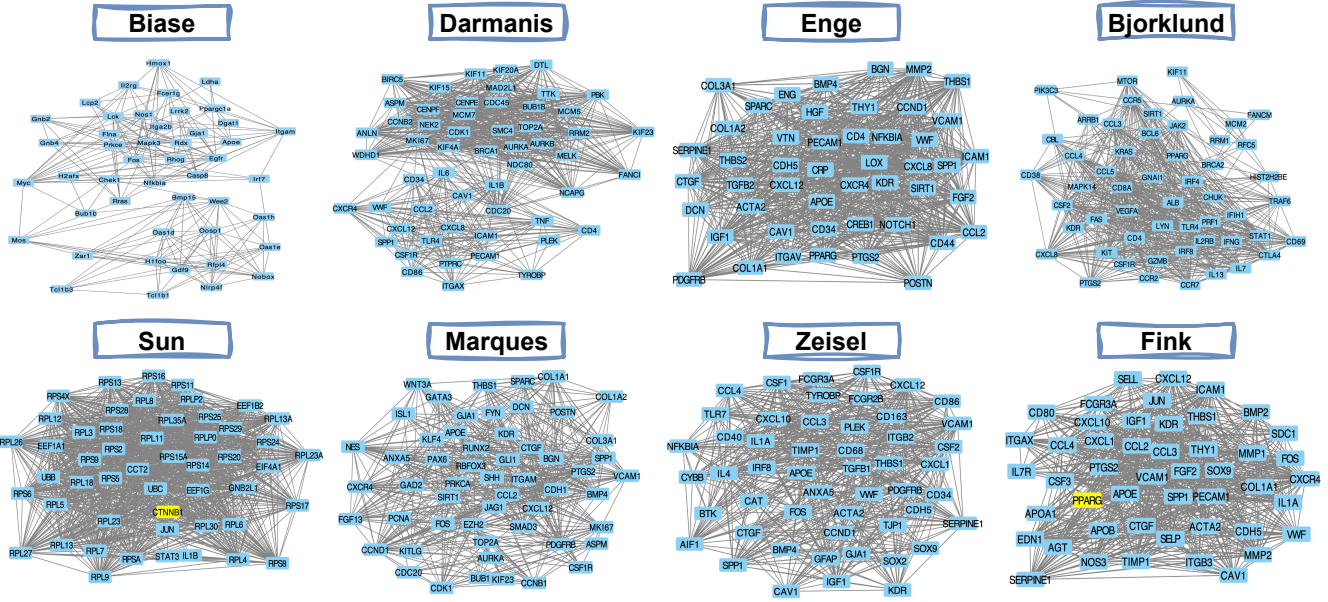


Fig. 4. Gene-to-gene graph of eight datasets.

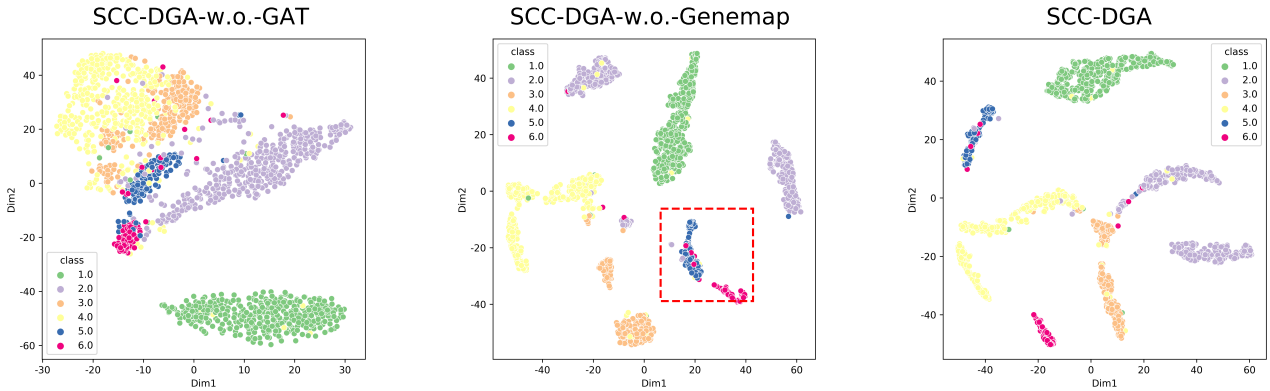


Fig. 5. Visualization of cell embeddings in dataset Sun.

To determine the optimal weight partitioning, we conducted experiments on four different datasets: Enge, Darmanis, Bjorklund, and Sun. And we have tested different values of λ . A smaller λ value indicates that the weight occupied by the cell graph is relatively small, while a larger λ value implies that the weight occupied by the gene graph is relatively small.

Figure 6 shows the clustering performance of SCC-DGA with different λ values. Our findings suggest that balanced dual-graph weights are crucial for improving clustering embeddings, with a λ value of 0.5 consistently producing excellent performance across all datasets.

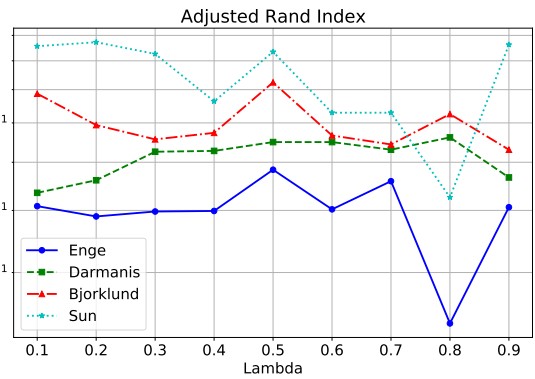


Fig. 6. Investigating optimal values for hyperparameter λ

E. Ablation study

The dual-graph alignment module is the key to our SCC-DGA model, relying on the cell-to-cell graph and gene-to-gene graph. And the cell-to-cell graph is built by a GAT module. To

TABLE III
ABLATION EXPERIMENTS ON SCC-DGA.

Dataset	Ours-w.o.-GAT	Ours-w.o.-Genemap	Ours
Biase	0.983	1.000	1.000
Darmanis	0.443	0.500	0.549
Enge	0.077	0.189	0.483
Bjorklund	-	0.513	0.724
Sun1	0.282	0.736	0.834
Marques	0.235	-	0.399
Zeisel	0.246	0.293	0.605
Fink	0.110	-	0.561

explore the impact of these modules on the clustering results, we conducted ablation experiments.

Specifically, we designed two additional variants based on SCC-DGA, which removed either the GAT module or the gene graph module. We compared their performance with the full SCC-DGA model, observing their clustering performance.

As shown in Table 3, SCC-DGA achieved the best clustering performance. If we removed the GAT module, the performance of the model decreased significantly, indicating the importance of the cell-to-cell network and its critical role in clustering. Although removing the gene map module did not result in as much decline in clustering performance, there was still a significant decrease, highlighting the crucial role of the gene graph in the clustering process. The fusion of both graphs produced the best performance, indicating that our dual-graph alignment module can effectively and stably enhance clustering.

IV. CONCLUSION

In conclusion, we developed an effective clustering model for scRNA data, SCC-DGA, which utilizes a dual-graph alignment module to constrain the cell-to-cell graph and gene-to-gene graph. The dual-supervised optimization module optimizes the cluster embeddings while maintaining the stability of both graphs during the optimization process. Our experimental results demonstrate that the cell-to-cell graph and gene-to-gene graph effectively enhance the optimization of embeddings, and our proposed model outperforms other existing methods.

Moving forward, we plan to explore novel methods for random walks on the gene-to-gene graph to obtain more effective representations. We also intend to investigate additional similarity measures of cells to construct a more accurate cell-to-cell graph [28], [29], [30], [31], [32]. Collaborative training is another promising avenue for future research, and we believe that the integration of cells and genes can enhance each other's effectiveness in clustering [33], [34].

REFERENCES

- [1] Dongqing Sun, Jin Wang, Ya Han, Xin Dong, Jun Ge, Rongbin Zheng, Xiaoying Shi, Binbin Wang, Ziyi Li, Pengfei Ren, et al. Tisch: a comprehensive web resource enabling interactive single-cell transcriptome visualization of tumor microenvironment. *Nucleic acids research*, 49(D1):D1420–D1430, 2021.
- [2] Lihong Peng, Feixiang Wang, Zhao Wang, Jingwei Tan, Li Huang, Xiongfei Tian, Guangyi Liu, and Liqian Zhou. Cell–cell communication inference and analysis in the tumour microenvironments from single-cell transcriptomics: data resources and computational strategies. *Briefings in Bioinformatics*, 23(4):bbac234, 2022.
- [3] Yunbin Zhang, Jingjing Song, Zhongwei Zhao, Mengxuan Yang, Ming Chen, Chenglong Liu, Jiansong Ji, and Di Zhu. Single-cell transcriptome analysis reveals tumor immune microenvironment heterogeneity and granulocytes enrichment in colorectal cancer liver metastases. *Cancer letters*, 470:84–94, 2020.
- [4] Sheng Hu Qian, Meng-Wei Shi, Dan-Yang Wang, Justin M Fear, Lu Chen, Yi-Xuan Tu, Hong-Shan Liu, Yuan Zhang, Shuai-Jie Zhang, Shan-Shan Yu, et al. Integrating massive rna-seq data to elucidate transcriptome dynamics in drosophila melanogaster. *Briefings in Bioinformatics*, page bbad177, 2023.
- [5] Qiao Liu, Wanwen Zeng, Wei Zhang, Sicheng Wang, Hongyang Chen, Rui Jiang, Mu Zhou, and Shaoting Zhang. Deep generative modeling and clustering of single cell hi-c data. *Briefings in Bioinformatics*, 24(1):bbac494, 2023.
- [6] Jiaqian Yan, Ming Ma, and Zhenhua Yu. bmvae: a variational autoencoder method for clustering single-cell mutation data. *Bioinformatics*, 39(1):btac790, 2023.
- [7] Peijie Lin, Michael Troup, and Joshua WK Ho. Cidr: Ultrafast and accurate clustering through imputation for single-cell rna-seq data. *Genome biology*, 18(1):1–11, 2017.
- [8] Vladimir Yu Kiselev, Kristina Kirschner, Michael T Schaub, Tallulah Andrews, Andrew Yiu, Tamir Chandra, Kedar N Natarajan, Wolf Reik, Mauricio Barahona, Anthony R Green, et al. Sc3: consensus clustering of single-cell rna-seq data. *Nature methods*, 14(5):483–486, 2017.
- [9] Guo Mao, Zhengbin Pang, Ke Zuo, and Jie Liu. Gene regulatory network inference using convolutional neural networks from scrna-seq data. *Journal of Computational Biology*, 30(5):619–631, 2023.
- [10] Xingyan Liu, Qunlun Shen, and Shihua Zhang. Cross-species cell-type assignment from single-cell rna-seq data by a heterogeneous graph neural network. *Genome Research*, 33(1):96–111, 2023.
- [11] Xiangjie Li, Kui Wang, Yafei Lyu, Huize Pan, Jingxiao Zhang, Dwight Stambolian, Katalin Susztak, Muredach P Reilly, Gang Hu, and Mingyao Li. Deep learning enables accurate clustering with batch effect removal in single-cell rna-seq analysis. *Nature communications*, 11(1):2338, 2020.
- [12] Tian Tian, Ji Wan, Qi Song, and Zhi Wei. Clustering single-cell rna-seq data with a model-based deep learning approach. *Nature Machine Intelligence*, 1(4):191–198, 2019.
- [13] Rahul Satija, Jeffrey A Farrell, David Gennert, Alexander F Schier, and Aviv Regev. Spatial reconstruction of single-cell gene expression data. *Nature biotechnology*, 33(5):495–502, 2015.
- [14] Juexin Wang, Anjun Ma, Yuzhou Chang, Jianting Gong, Yuexu Jiang, Ren Qi, Cankun Wang, Hongjun Fu, Qin Ma, and Dong Xu. scgcn is a novel graph neural network framework for single-cell rna-seq analyses. *Nature communications*, 12(1):1882, 2021.
- [15] Yi Cheng and Xiuli Ma. scgac: a graph attentional architecture for clustering single-cell rna-seq data. *Bioinformatics*, 38(8):2187–2193, 2022.
- [16] Dayu Hu, Ke Liang, Sihang Zhou, Wenxuan Tu, Meng Liu, and Xinwang Liu. scdfc: A deep fusion clustering method for single-cell rna-seq data. *Briefings in Bioinformatics*, page bbad216, 2023.
- [17] Fernando H Biase, Xiaoyi Cao, and Sheng Zhong. Cell fate inclination within 2-cell and 4-cell mouse embryos revealed by single-cell rna sequencing. *Genome research*, 24(11):1787–1796, 2014.
- [18] Spyros Darmanis, Steven A Sloan, Ye Zhang, Martin Enge, Christine Caneda, Lawrence M Shuer, Melanie G Hayden Gephart, Ben A Barres, and Stephen R Quake. A survey of human brain transcriptome diversity at the single cell level. *Proceedings of the National Academy of Sciences*, 112(23):7285–7290, 2015.
- [19] Martin Enge, H Efsun Arda, Marco Mignardi, John Beausang, Rita Bottino, Seung K Kim, and Stephen R Quake. Single-cell analysis of human pancreas reveals transcriptional signatures of aging and somatic mutation patterns. *Cell*, 171(2):321–330, 2017.
- [20] Åsa K Björklund, Marianne Forkel, Simone Picelli, Viktoria Konya, Jakob Theorell, Danielle Friberg, Rickard Sandberg, and Jenny Mjösberg. The heterogeneity of human cd127+ innate lymphoid cells revealed by single-cell rna sequencing. *Nature immunology*, 17(4):451–460, 2016.
- [21] Zhe Sun, Li Chen, Hongyi Xin, Yale Jiang, Qianhui Huang, Anthony R Cillo, Tracy Tabib, Jay K Kolls, Tullia C Bruno, Robert Lafyatis, et al. A bayesian mixture model for clustering droplet-based single-cell transcriptomic data from population studies. *Nature communications*, 10(1):1649, 2019.
- [22] Sueli Marques, David van Bruggen, Darya Pavlovna Vanichkina, Elisa Mariagrazia Floriddia, Hermany Munguba, Leif Våremo, Stefania Giacomello, Ana Mendanha Falcao, Mandy Meijer, Åsa Kristina Björklund, et al. Transcriptional convergence of oligodendrocyte lineage

- progenitors during development. *Developmental cell*, 46(4):504–517, 2018.
- [23] Amit Zeisel, Ana B Muñoz-Manchado, Simone Codeluppi, Peter Lönnerberg, Gioele La Manno, Anna Juréus, Sueli Marques, Hermany Munguba, Liqun He, Christer Betsholtz, et al. Cell types in the mouse cortex and hippocampus revealed by single-cell rna-seq. *Science*, 347(6226):1138–1142, 2015.
- [24] Emily E Fink, Surbhi Sona, Uyen Tran, Pierre-Emmanuel Desprez, Matthew Bradley, Hong Qiu, Mohamed Eltemamy, Alvin Wee, Madison Wolkov, Marlo Nicolas, et al. Single-cell and spatial mapping identify cell types and signaling networks in the human ureter. *Developmental Cell*, 57(15):1899–1916, 2022.
- [25] Lawrence Hubert and Phipps Arabie. Comparing partitions. *Journal of classification*, 2:193–218, 1985.
- [26] Alexander Strehl and Joydeep Ghosh. Cluster ensembles—a knowledge reuse framework for combining multiple partitions. *Journal of machine learning research*, 3(Dec):583–617, 2002.
- [27] Peter J Rousseeuw. Silhouettes: a graphical aid to the interpretation and validation of cluster analysis. *Journal of computational and applied mathematics*, 20:53–65, 1987.
- [28] Hong Wang, Xiaoyan Lu, Hwei Zheng, Wencan Wang, Guosi Zhang, Siyu Wang, Peng Lin, Youyuan Zhuang, Chong Chen, Qi Chen, et al. Rnasmc: A integrated tool for comparing rna secondary structure and evaluating allosteric effects. *Computational and Structural Biotechnology Journal*, 2023.
- [29] Shixiong Zhang, Xiangtao Li, Jiecong Lin, Qiuzhen Lin, and Ka-Chun Wong. Review of single-cell rna-seq data clustering for cell-type identification and characterization. *RNA*, 29(5):517–530, 2023.
- [30] Michelle Ying Ya Lee, Klaus H Kaestner, and Mingyao Li. Benchmarking algorithms for joint integration of unpaired and paired single-cell rna-seq and atac-seq data. *bioRxiv*, pages 2023–02, 2023.
- [31] Taiyun Kim, Irene Rui Chen, Yingxin Lin, Andy Yi-Yang Wang, Jean Yee Hwa Yang, and Pengyi Yang. Impact of similarity metrics on single-cell rna-seq data clustering. *Briefings in bioinformatics*, 20(6):2316–2326, 2019.
- [32] Mei Li, Ya-Wen Zhang, Ze-Chang Zhang, Yu Xiang, Ming-Hui Liu, Ya-Hui Zhou, Jian-Fang Zuo, Han-Qing Zhang, Ying Chen, and Yuan-Ming Zhang. A compressed variance component mixed model for detecting qtns and qtn-by-environment and qtn-by-qtn interactions in genome-wide association studies. *Molecular Plant*, 15(4):630–650, 2022.
- [33] Tien-Phat Nguyen, Trong-Thang Pham, Tri Nguyen, Hieu Le, Dung Nguyen, Hau Lam, Phong Nguyen, Jennifer Fowler, Minh-Triet Tran, and Ngan Le. Embryosformer: Deformable transformer and collaborative encoding-decoding for embryos stage development classification. In *Proceedings of the IEEE/CVF Winter Conference on Applications of Computer Vision*, pages 1981–1990, 2023.
- [34] Jean Ogier du Terrail, Armand Leopold, Clément Joly, Constance Béguier, Mathieu Andreux, Charles Maussion, Benoît Schmauch, Eric W Tramel, Etienne Bendjebbar, Mikhail Zaslavskiy, et al. Federated learning for predicting histological response to neoadjuvant chemotherapy in triple-negative breast cancer. *Nature Medicine*, pages 1–12, 2023.